Research Article Vol. 28, No. 4 / 17 February 2020 / Optics Express 5459
Optics EXPRESS

Control of quantum dot emission by colloidal plasmonic pyramids in a liquid crystal

HARIDAS MUNDOOR,[1] ENID M. CRUZ-COLÓN,[1] SUNGOH PARK,[1] QINGKUN LIU,[1] IVAN I. SMALYUKH,[1,2,3,5] AND JAO VAN DE LAGEMAAT[3,4,6]

[1]*Department of Physics and Soft Material Research Center, University of Colorado Boulder, Boulder, CO 80309, USA*
[2]*Department of Electrical, Computer, and Energy Engineering, Materials Science and Engineering Program, University of Colorado, Boulder, CO 80309, USA*
[3]*Renewable and Sustainable Energy Institute, National Renewable Energy Laboratory and University of Colorado, Boulder, CO 80309, USA*
[4]*National Renewable Energy Laboratory, Golden, CO 80401, USA*
[5]*ivan.Smalyukh@colorado.edu*
[6]*jao.vandelagemaat@nrel.gov*

Abstract: We study the plasmon-enhanced fluorescence of a single semiconducting quantum dot near the apex of a colloidal gold pyramid spatially localized by the elastic forces of the liquid crystal host. The gold pyramid particles were manipulated within the liquid crystal medium by laser tweezers, enabling the self-assembly of a semiconducting quantum dot dispersed in the medium near the apex of the gold pyramid, allowing us to probe the plasmon-exciton interactions. We demonstrate the effect of plasmon coupling on the fluorescence lifetime and the blinking properties of the quantum dot. Our results demonstrate that topological defects around colloidal particles in liquid crystal combined with laser tweezers provide a platform for plasmon exciton interaction studies and potentially could be extended to the scale of composite materials for nanophotonic applications.

1. Introduction

Emission control of single-particle fluorescence using metal nanoparticle is a topic of rapidly increasing scientific importance and technological relevance [1–6]. The interest in this field stems from potential applications in a wide range of areas, such as optical communications, imaging, solar energy conversion, display devices, sensors, etc. [7–9]. Since the optical interactions occur within subwavelength distances, these studies are often challenged by the fabrication methods used for assembling nanoparticles into configurations with distances and geometry optimal to probe the interaction. Although the experimental methods utilizing lithography and scanning probe-based techniques have been used extensively for these studies, they are often limited by the high cost and relatively slow preparation process [10,11]. On the other hand, self-assembly using soft materials emerged as a versatile and efficient method for assembling nanoparticles into the predesigned configuration with nanometer-scale precision. Soft materials such as polymers, polyelectrolytes, biopolymers, and DNA have been used efficiently for the nanoparticle self-assembly [12–14]. It has been demonstrated that the hierarchical organization of semiconducting quantum dot (QD) and metal nanoparticles can be prepared by using block copolymer templated assembly, where the nanoparticles are segregated into separate blocks of the polymer template, depending on the surface chemical properties of the particles [12]. Recently, we have demonstrated that the self-assembled structures of molecular alignment in liquid crystal (LC) materials could be used for controlled nanoscale optical interaction studies [4,6]. LCs are highly anisotropic materials with long-range orientational order and fluid-like

#383672 https://doi.org/10.1364/OE.383672
Journal © 2020 Received 20 Nov 2019; revised 23 Jan 2020; accepted 25 Jan 2020; published 12 Feb 2020

Optics EXPRESS

behavior which produces elastic distortions and topological defects, allowing for pre-defined nanoscale self-assembly of colloidal inclusions within the LC medium [11,15–18]. Moreover, the highly reconfigurable properties of LC materials can be controlled through external stimuli such as electric and magnetic fields, providing much-needed control over the optical interactions through the tunable inter-particle spacing between the nanoparticles.

In this work, we demonstrate how colloidal particles can self-assemble within the bulk of a nematic LC to provide a toolkit for probing plasmon-exciton interactions. This self-assembly is driven by the minimization of the free energy of the LC host, allowing for the spontaneous well-defined relative arrangement of particles needed to probe the effect of the plasmonic enhancement on the physical behavior of a single fluorescent QD particle. The gold micro pyramid (GMP) particles dispersed in the LC medium self-assemble with high-index (made of melamine resin) dielectric colloidal spheres to effectively form a colloidal dimer with GMP-based plasmonic metal tip that can be manipulated in a holonomic way with the help of optical tweezers by moving the sphere attached at the base of the gold pyramid. The surface topological LC defect (called "boojum") at the tip of the GMP elastically entraps QDs near its apex, allowing us to probe the fluorescence properties of the particles under strong plasmon exciton coupling. We show how plasmon-exciton interactions in this hybrid GMP-QD colloidal system alter fluorescence intermittency and luminescence lifetime. By analyzing the emission characteristics of the QD trapped at the apex of the GMP with the help of time-resolved spectroscopy techniques, we demonstrate strong plasmon-exciton coupling and discuss how the combination of colloidal self-assembly and plasmon-exciton interactions can be useful for the preparation of next-generation photonic materials and devices utilizing metal and semiconductor nanoparticles.

2. Experimental techniques and materials

2.1. Preparations of GMPs and LC colloids

Colloidal GMPs used in the experiments were prepared using photolithography and film deposition followed by controlled chemical etching in a dilute sodium hydroxide (NaOH) as reported earlier [19,20]. GMPs are hollow pyramids without the base and having a base length of 3.7 μm and shell thickness 200 nm, as illustrated by the scanning electron micrograph (SEM) depicted in Fig. 1(a). The GMPs were functionalized with thiol terminated polyethylene glycol (PEG), which promote tangential boundary conditions for the LC molecules at the GMP surfaces. We used commercially available CdSe/ZnS core-shell QDs (Ocean Nanotech) with a 10 nm CdSe core and a ZnS shell showing an emission peak at 620 nm. Owing to their core-shell geometry, the QDs were characterized with high quantum efficiency and showed excellent photostability under continuous laser excitation and re-dispersion in different media like solvents and LCs. The melamine resin spheres (purchased from Duke Scientific) were characterized with a diameter of 7 μm and used without any further surface functionalization. Due to the relatively high index of refraction (1.69), the melamine resin sphere can be manipulated in the LC medium using the trapping system. To prepare LC colloidal dispersions, we mixed dilute dispersions of the colloidal particles in ethanol or toluene with 4-cyano-4'-pentylbiphenyl (5CB). The particle concentrations in the respective solvents were determined by drop coating a known volume of colloidal dispersion onto a glass substrate followed by imaging the drop coated area using the optical microscope to estimate the total number of particles in the solution volume. The desired particle concentrations in the LC medium were achieved by mixing the required volume of colloidal dispersions with LC. The LC mixtures were kept at 70°C for 2 h to evaporate the solvents and subsequently quenched to nematic phase under vigorous mechanical agitation. To prevent the aggregation during solvent evaporation, the colloidal dispersions of GMPs, QDs and melamine resin spheres were prepared separately. The dispersions were infiltrated into a glass cell with a spacing of 16 μm and sealed with a fast setting epoxy. To promote the tangential

Optics EXPRESS

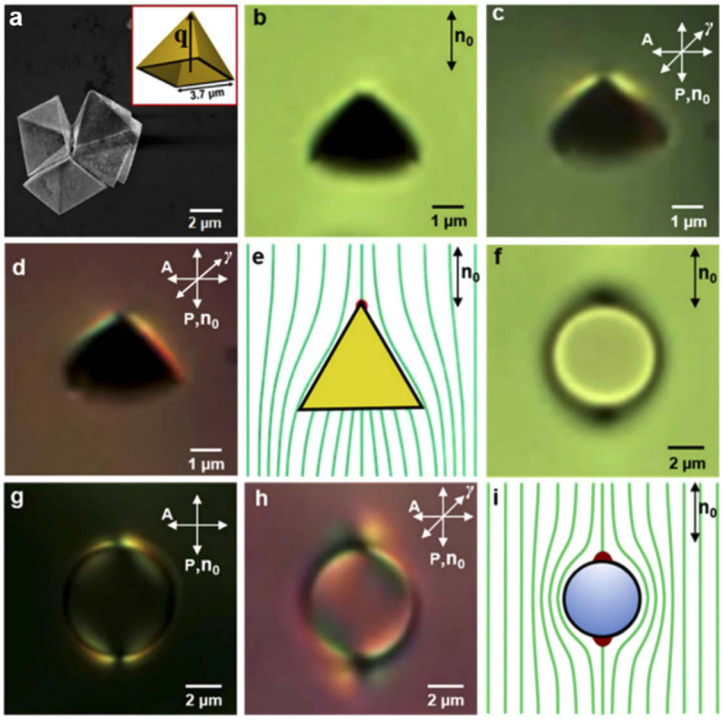

Fig. 1. Colloidal building blocks of GMP-based tip with holonomic control. (a) SEM micrograph of GMPs cluster on a silicon surface. The inset shows a schematic of a GMP with the particle dimensions and base to tip vector **q**. (b-d) Optical micrographs of a GMP dispersed in LC, as obtained in bright field (b) and polarizing imaging modes without (c) and with retardation plate (d). (e) Schematic representation of the director configuration around a GMP, showing the boojum (red filled disc) and the far-field director $\mathbf{n_0}$. Note that there is also a boojum (not shown) in the interior of the pyramid [19]. (f-g) Optical micrographs of a melamine resin sphere dispersed in LC obtained in brightfield (f), and polarizing imaging modes without (g) and with (h) a retardation plate. (i) Schematic representation of director configuration around a melamine resin sphere with tangential boundary conditions, showing $\mathbf{n_0}$ and two boojum surface defects.

unidirectional alignment of the LC molecules at the surface of glass substrates, we coated the inner surface of glass plates with polyvinyl alcohol (PVA) and then rubbed them unidirectionally.

2.2. Optical measurements methods and materials

Optical characterizations of the colloidal particles dispersed in LC medium were performed on an inverted optical microscope (Olympus IX 81), equipped with a holographic optical tweezer (HOT), light sources, polarizers, high magnification objectives, and a CCD camera (Flea-COL, PointGrey) for imaging. The HOT system utilizes the 1064 nm output from a fiber laser (IPG photonics) and a spatial light modulator (SLM) to produce multiple independent traps in the sample space. The optical microscopy images of the GMPs and melamine resin spheres dispersed in the LC medium were collected using a 100x oil immersion objective (Olympus, UPlanSApo, NA = 1.42) under white light illumination, while the QDs were imaged using their fluorescence signal when illuminated with a 436 nm light from a mercury lamp. To characterize the fluorescence blinking of QDs, we focused a 473 nm linearly polarized continuous wave (CW) output from a solid-state laser (Laserglow Technologies) onto the sample using the 100x oil immersion objective and

Optics EXPRESS

fluorescence signal from the QDs were collected by the same objective and recorded by an avalanche photodiode (APD) connected to a data acquisition board (NIDAQ-6363, National Instruments) and analyzed using a homebuilt MATLAB code. The fluorescence decay and photon antibunching characterization of the QDs fluorescence were performed using the same setup with slight modifications. For the fluorescence decay measurements, the QDs were excited using the 467 nm linearly polarized pulsed output from a diode laser (Nano LED- Horiba Scientific, 1 MHz, 200 ps) and the fluorescence signal detected by the APD was sent to a time-correlated single-photon counting hardware (TCSPC, SPC 130, Becker and Heckle) for further processing. Photon antibunching measurements were also performed under 473 nm linearly polarized CW laser excitation and the fluorescence signals from the QDs were analyzed using a Hanbury Brown-Twiss interferometer set-up. Within this setup, the fluorescence signal collected by the objective was split into two APDs using a 50/50 beam splitter and the coincidence counts between the photons arriving at the APDs were repeatedly measured with high temporal resolution, using the TCSPC hardware. The polarization state of the excitation beam was kept parallel to the far field director $\mathbf{n_0}$.

2.3. Numerical simulations

The simulations of electric field enhancement due to GMPs were performed using the COMSOL Multiphysics software. The pyramidal gold structures of GMPs were generated using the drawing tool in COMSOL, which were enclosed between perfectly matched layers on all sides to account for the boundary conditions. The simulations were performed assuming the standard refractive index values of gold and a constant refractive index value ($\eta = 1$) for the medium. Due to computational limitations, the simulations for a single GMP were done for smaller particle size, with the base length of 2 μm, a factor of two smaller than what was used in experiments. For calculations involving four GMP assembly, the particle dimensions were reduced by a factor of 8. We then calculated the field intensity enhancement $\frac{|E|^2}{|E_0|^2}$ due to the GMPs at 620 nm, where E is the enhanced electric field component due to the GMPs and E_0 is the electric field component of the incident light.

3. Results and discussion

When dispersed in LC, the studied GMPs spontaneously orient with their base to apex vector $\mathbf{q}$ parallel to the far-field director $\mathbf{n_0}$, [19] as illustrated in Figs. 1(b)–1(e). In response to the tangential boundary conditions of the GMPs, the LC with the far-field director $\mathbf{n_0}$ becomes distorted near the GMPs, resulting in the localized director structures of $\mathbf{n(r)}$, which are visible in the polarized microscopy images shown in Figs. 1(c) and 1(d). The spontaneous alignment of GMPs relative to $\mathbf{n_0}$ is a result of the minimization of free energy of the elastic distortions, which is achieved for the observed orientations of colloidal GMPs. The energy-minimizing director distortions around a GMP dispersed in LC are schematically represented in Fig. 1(e). The analysis of symmetry breaking indicates a dipolar elastic structure of the distortions around these particles [21]. The free energy minimization under these surface boundary conditions for the LC molecules create a topological defect called "boojums" very close to the apex of the pyramid, which is visible as a dark spot in the polarized optical microscopy images (Figs. 1(c) and 1(d)) and marked red in the schematic shown in Fig. 1(e). Owing to the minimization of elastic free energy cost, the small nanoparticles dispersed in the LC medium are attracted into boojums, being trapped by the elastic forces [22], providing an ideal platform for studying the optical interaction between the GMPs and a QD as illustrated below. The GMPs can be manipulated in the LC medium with the help of an optical trapping system by moving the focused laser beam of the laser tweezers. However, the control of particle orientation and movement by the laser tweezer is somewhat limited due to the melting of LC medium surrounding the GMPs

Optics EXPRESS

due to the strong absorption of the focused infrared beam used for optical trapping when focused directly on the gold GMP. To overcome these limitations, we have utilized elasticity-mediated colloidal self-assembly [23] and effectively attached a melamine resin sphere at the base of GMPs and the particles are moved inside the LC medium by using the melamine resin spheres as a handle, enabling effective holonomic control of both orientations and positions of the GMP. The melamine resin sphere shows tangential surface alignment with two surface point defects (boojums) located at the top and bottom of the sphere (Figs. 1(f)–1(i)). The polarized microscopy images reveal the director distortion around the melamine resin particles due to the surface of the particle with tangential boundary conditions, indicating the quadrupolar nature of elastic distortions as illustrated in Fig. 1(i). When co-dispersed in the LC, the GMPs and melamine resin spheres interact attractively along the far-field director $\mathbf{n_0}$, due to the dipolar - quadrupolar elasticity-mediated interactions between the particles [19]. Figures 2(a)–2(d) illustrates the attractive interaction between a GMP and a melamine resin sphere, represented by the optical images collected at different instances during the self-assembly process. The $\mathbf{n(r)}$ distortions around the self-assembled structure are revealed in the polarized optical microscopy images in Figs. 2(e) and 2(f), which can be represented schematically as shown in Fig. 2(g). The exterior of the GMP-melamine resin sphere assembly shows two boojums located at the top and bottom of the colloidal structure. Once assembled, the GMP and the melamine resin form a stable colloidal dimer-like assembly, since they are held together by the strong elastic forces, mediated by the LC host medium.

The self-assembled colloidal structure of GMP and melamine resin sphere can be manipulated in the LC using the HOT system, by utilizing the optical forces acting on the melamine resin sphere, which allows us to controllably probe the optical interaction between the GMPs and QDs dispersed within the LC. Owing to the strong plasmonic field enhancement (Fig. 2(h)), the QD particles elastically trapped near the apex of the pyramid showed a substantial modification of their emission properties, which we characterize as detailed below. Furthermore, the attractive elastic interactions due to the dipolar elastic distortions around the GMPs allow for the controlled self-assembly of nanoparticles in the LC medium, as illustrated in Fig. 2(i). The particles can be assembled by bringing the GMPs close to each other using the HOT system and releasing them at the close proximity ($\sim 10\,\mu$m) allowing them to interact by the LC mediated elastic forces. For instance, Fig. 2(i) shows the optical micrograph of a four-GMP assembly formed in the LC medium and an idealized colloidal structure of the particle assembly can be represented schematically as shown in Fig. 2(j). The particle assembly depicted in Fig. 2(j) allows for interparticle plasmon coupling between GMPs resulting in substantially enhanced electric field intensity at the center of the assembled structure [24,25]. The electromagnetic simulations (Figs. 2(h) and 2(k)) indicate a $\sim$ 6-fold enhancement in the electric field intensity at the center of the GMP assembly compared to the maximum field enhancement near the apex of a single GMP at 620 nm.

To investigate the effect of plasmon coupling due to GMPs on the photophysics of a single QD, we prepared separate colloidal dispersions of QDs and GMPs in 5CB. To prevent aggregation and to ensure single QD dispersions, the concentration of QDs in 5CB was kept very low (0.8–1.2 QD per μm^3). The dispersions of QDs and GMPs were infiltrated into a glass cell with planar surface boundary conditions and inspected with the help of an inverted microscope, while optically exciting the QDs in the LC medium using the 436 nm light from a mercury lamp. We located a GMP particle and moved it through the LC medium using the HOT system until a single QD particle became trapped in the boojum near the apex of the GMP (Figs. 3(a) and 3(b)). To analyze the QD emission, we focused a 473 nm CW laser into the apex of the pyramid and a fluorescence time trace of the QD emission was recorded using an APD, with a binning time of 10 ms. The particle showed fluorescence blinking typical of QD emission, but at a faster rate compared to the fluorescence emission from a QD located at the glass substrate of the confining cell as illustrated

Optics EXPRESS

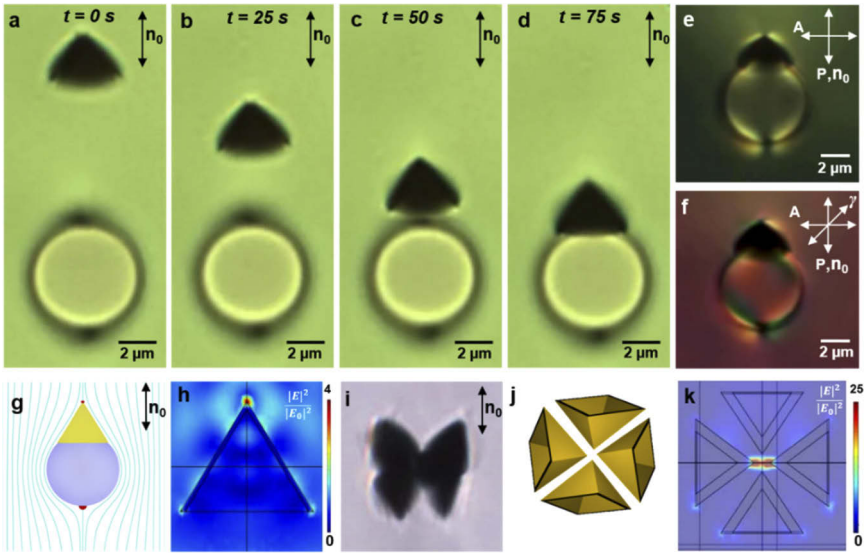

Fig. 2. Colloidal plasmonic superstructures fabricated through self-assembly. (a-d) Experimental sequence of optical micrographs, with elapsed time showing the assembly of a GMP and melamine resin sphere dispersed in LC. The final assembled colloidal structure is shown in (d). (e,f) Optical micrograph of the GMP-melamine sphere assembly obtained in polarized imaging mode without (e) and with (f) retardation plate. (g) Schematic representation of **n(r)** distortions around GMP-melamine resin sphere assembly showing far field director $\mathbf{n_0}$ and two boojums (marked in red). (h) Electric field intensity enhancement map around a GMP at 620 nm simulated using COMSOL Multiphysics. (i) Optical micrograph of the colloidal structure formed by the assembly of GMPs in LC obtained under brightfield microscopy. (j) Schematic representation of an idealized colloidal structure that could be used for plasmonic enhancement beyond what is accessible to a single pyramid; we note that the actual structure of multi-GMP assembly shown in (i) is somewhat different from this idealized assembly due to the complexity of elasticity-mediated interactions, though showing the general principle of how elastic interactions could be used to guide colloidal assembly for these purposes. (k) Electric field intensity enhancement map at 620 nm due to the colloidal assembly of four GMPs in the geometry shown by the schematic in (j).

in Fig. 4. The QD on the glass substrate showed prolonged "off" times between the fluorescence emission (Fig. 4(a)), which can be quantified using the histogram shown in Fig. 4(c). On the other hand, the QD fluorescence near the apex of a GMP showed an increased prevalence of "on" time as illustrated by the plots in Figs. 4(b) and 4(d). The analysis of the probability distribution of the "on" and "off" times (t_{on} and t_{off}) of the QD fluorescence, based on constant thresholding method reveals the typical power-law dependence indicating that the QD emission follows a Poissonian photon distribution as reported earlier [26]. The slight increase in the photon counts for the QD fluorescence near apex of GMPs can be attributed to the change in radiation pattern of the QD fluorescence due to the antenna like arrangement leading to a preferential beaming of emission light into the microscope objective [27]. The measurements were repeated on multiple GMP-QD assemblies and the observed variations in the blinking properties of the QDs were found to be highly reproducible. From these observations, it is evident that the GMPs modify the blinking of the QD fluorescence, by channeling the excitation energy to radiative process rather than decaying through the nonradiative process. Further insight into the plasmon exciton interaction can be gleaned from the analysis of radiative decay rates of the QD fluorescence obtained by fitting a double exponential curve to the fluorescence decay as illustrated in Fig. 3(c).

Optics EXPRESS

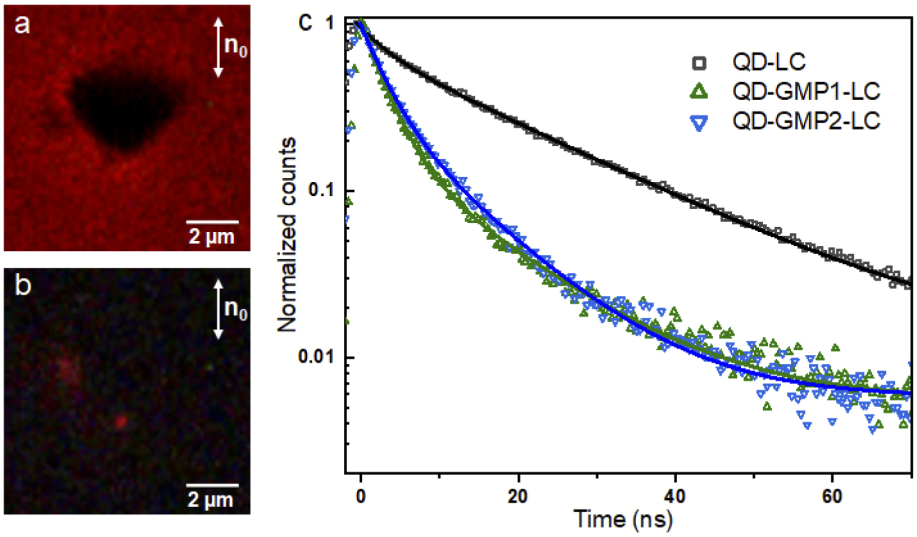

Fig. 3. Plasmonic effects on QD fluorescence. (a,b) Optical micrograph of a GMP dispersed in LC with a QD elastically trapped near the apex when viewed with a red filter under white light illumination (a) and with 473 nm excitation showing the fluorescence from QD (b). (c) Fluorescence decay curve from the QD located at the glass substrate (black square) of the confining cell and near the apex of a GMP dispersed in LC, representing typical fluorescence decay curves collected from two different GMP-QD assemblies (green and blue triangles). Solid curves represent exponential fit to the experimental data.

The emission decay of the single QD fluorescence from the glass substrate follows a single exponential curve with a decay time $\tau\sim$ 20 ns, which is the typical value of exciton lifetime for such a core-shell nanoparticle [4,28]. However, the fluorescence decay of the QD located at the apex of a GMP shows a double exponential decay, with average lifetimes $\tau_1 = 2.5$ ns and $\tau_2 = 8$ ns, indicating a three to 8 times enhancement in the radiative decay rates of the QD fluorescence, likely originating from the strong plasmon exciton interaction, due to the Purcell effect. The faster component in the QD fluorescence decay could arise from biexciton states of the QD emission owing to multiphoton absorption or from multiphoton emission as reported earlier [4]. Moreover, such observations are consistent for multiple GMP-QD assemblies (Fig. 3(c), compare the green and blue curves corresponding to different GMP-QD pairs).

In order to analyze the multiphoton emission from the QD located at the apex of a GMP, we analyzed the QD emission using a photon antibunching set up. Figure 5 represents the typical photon antibunching curves of the emission for the QD on the glass substrate and at the apex of GMP. The data is fit using the expression $g^{(2)}(t) = g^{(2)}(0) + (1 - e^{-\left|\frac{t}{\tau}\right|})/N$, where τ is the exciton lifetime, N is the number of photons and $g^{(2)}(0)$ is the second-order correlation at the coincidence time $t = 0$. For the data shown in Fig. 5(a), which corresponds to the QD fluorescence on glass substrate, we obtain $N = 1.1$, $g^{(2)}(0) = 0.15$ and $\tau = 21$ ns. Similar analysis of the antibunching curve for the QD emission from the apex of GMP (Fig. 5(b)) yields $N = 1.23$, $g^{(2)}(0) = 0.25$, and $\tau = 9$ ns. Both these results indicate single-photon emission property of the QDs, which also rules out the possible plasmon mediated multiphoton emission for the QD near the apex of GMP. However, the effect of plasmon exciton coupling is evident from the decreased exciton lifetime of the QD at the apex of the GMP extracted from the antibunching curve depicted in Fig. 5(b) as well as from the fluorescence decay curves (Fig. 3(c)). The observed variations in the optical

Optics EXPRESS

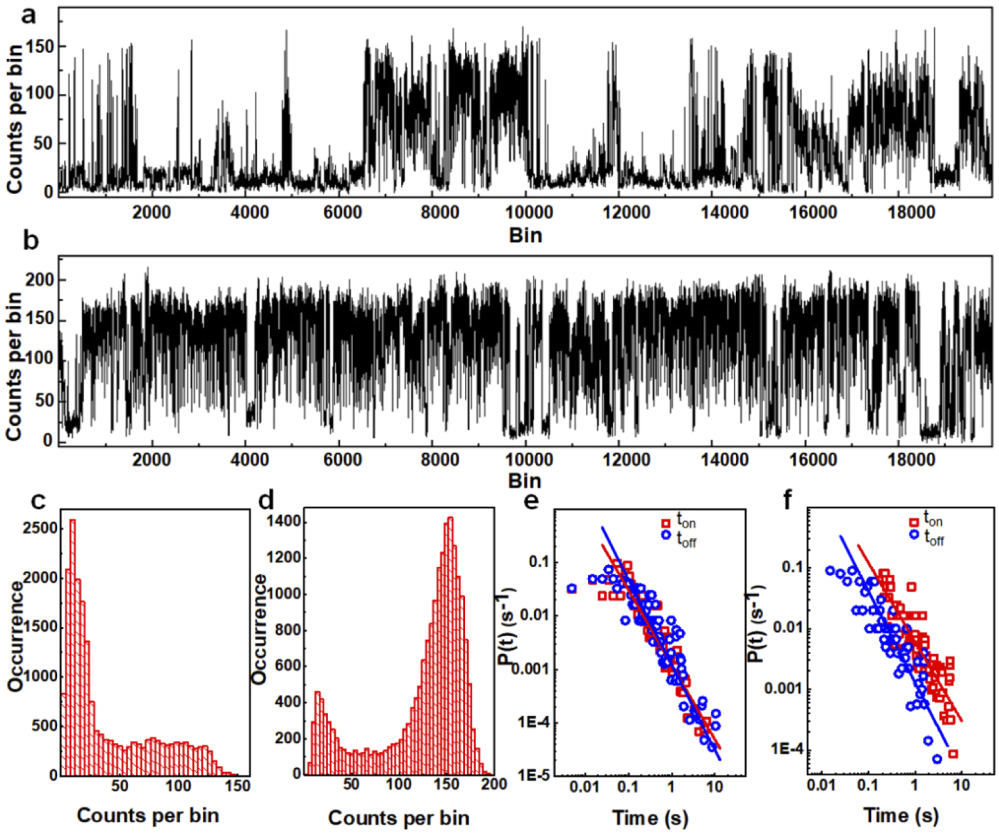

Fig. 4. Fluorescence intermittency of QD without and with the plasmonic enhancement. (a,b) Time trace of the single QD fluorescence, collected with a binning time of 10 ms, for a particle located at the glass substrate of the confining cell (a) and elastically tapped near the apex of the GMP (b). (c,d) Histogram showing the intensity variations of the QD fluorescence for the curves shown in (a) and (b) indicating the "on" and "off" times of the QD fluorescence. (e,f) The probability density analysis of QD fluorescence time traces based on the constant thresholding method representing the sustained "on" (t_{on}) and "off" (t_{off}) times for a QD located at the glass substrate (e) and at the apex of the GMP (f).

properties of the QDs near the apex of GMPs were found to be highly reproducible as verified by the several independent measurements on multiple QD-GMP assemblies.

Recently, we have reported evidence of multiphoton emission from a QD coupled to GNR dimer, elastically trapped within the LC line defect [4]. The dimer-like configuration of the GNRs used in the experiment induces strong plasmon exciton coupling, owing to the spectral overlap of QD fluorescence with the surface plasmon resonance (SPR) of the nanorod dimer. Although the electromagnetic simulations indicate a strong field intensity enhancement for GMPs at 620 nm, the field enhancement is relatively lower compared to the gold nanorod dimer configuration used in the earlier experiments [4]. The weaker field intensity enhancement for GMPs is the result of a large offset in the emission peak (620 nm) with respect to the SPR peak, which is reported to be in the near-infrared (~ 980 nm) part of the spectrum [29]. Our results from photon antibunching analysis indicate that the coupling of QD fluorescence with the GMPs is inadequate to induce sufficient modifications in the radiative decay of biexcitonic states of the QDs to enhance the quantum yield of the biexciton emission. Biexcitonic states apparently still decay through Auger

Optics EXPRESS

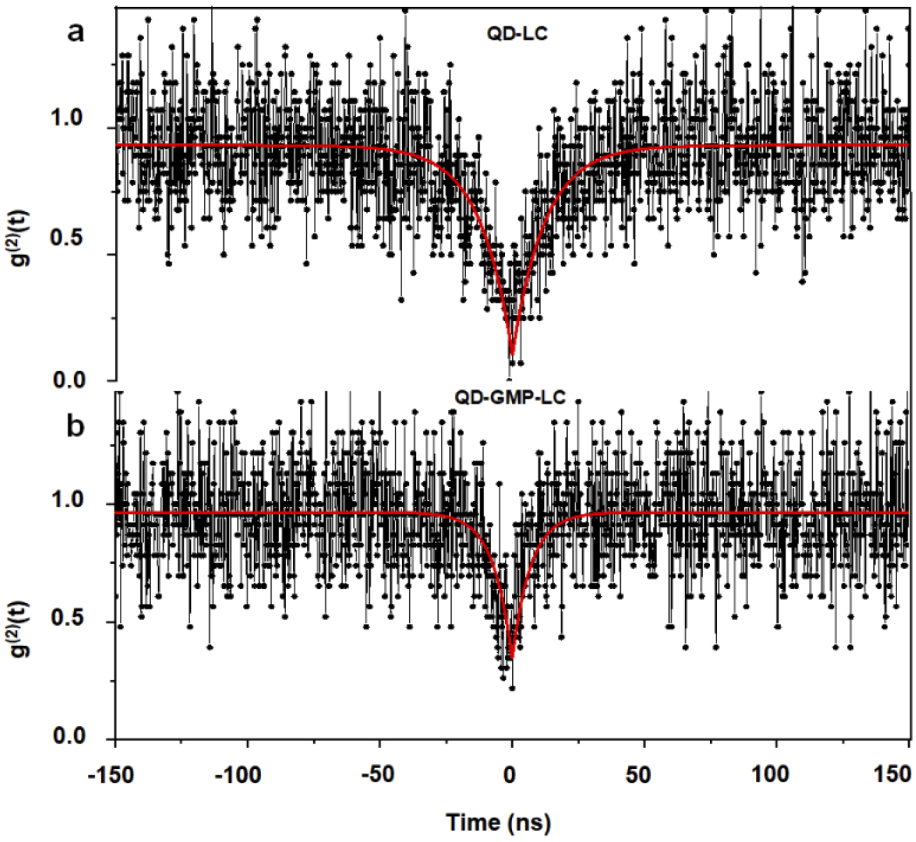

Fig. 5. Photon antibunching characterization of QD emission. Fluorescence antibunching curves of a single QD located at the surface of the glass substrate forming the LC cell (a) and elastically trapped near the apex of GMP dispersed in LC (b). Faster decay of the QD fluorescence is evident in (b) relative to (a), as revealed by the relatively sharper dip in the antibunching curve shown in (b). Solid lines represent fit to the experimental data.

and other non-radiative channels/mechanisms. On the other hand, the radiative decay rates corresponding to excitonic states of the QDs are enhanced by almost 3 times, as evident from the fluorescence decay measurements, which is consistent with our previous measurements [4]. The faster component in the fluorescence decay can be attributed to the trap states of the QD. The QDs can also transfer the excitation energy to the GMPs through nonradiative process, which is more prominent mode of energy transfer at the relatively short distance between particles resulting in the quenching of QD fluorescence [11]. The LC boojum defects have the handle-like geometric shape of singular cores [30] at the scale of the nematic coherence length (10-20 nm). These handles thus allow for the entrapment of QDs in the LC medium some ~10 nm away from the apex of GMPs, preventing the aggregations of QDs onto the surface of the gold particles, which would result in the complete quenching of QD fluorescence.

4. Conclusions

In conclusion, we have demonstrated the use of topological boojum defects nearby a colloidal particle dispersed in a LC to study the nanoscale optical interaction between a GMP and a single QD particle. We demonstrated the means to manipulate the gold colloidal particles as well as various geometries and configurations of colloidal structures that can be formed within the LC

Optics EXPRESS

medium by utilizing the elastic forces of interaction between them, which can be of interest to the study optical interaction at the nanoscale. While the use of plasmonic tips to probe the plasmon-exciton interactions is common, our work shows how such plasmonic tips can take the form of colloidal pyramids, which can be manipulated in a holonomic fashion by utilizing a combination of elasticity-mediated forces and laser trapping of high-index dielectric colloidal spheres co-self-assembled with these pyramids. Using this plasmonic enhancement tool, we have analyzed the optical properties of a single QD particle elastically trapped near the apex of a GMP using the time-resolved optical techniques and explained the results considering the plasmon exciton coupling. Since the elasticity-mediated colloidal interactions are long-ranged and extend to distances of about 10 μm [21,31], larger than all three types of used particles, one can envisage purely elastic hierarchical self-assembly based formation of desired colloidal superstructures. For example, one can envisage elasticity-mediated self-assembly of mesoscale crystals [31] formed by GMP-QD colloidal superstructures as building blocks, which would then lead to colloidal metamaterials with pre-designed properties stemming from the plasmon-exciton interactions. Moreover, elasticity-driven relative placement of plasmonic and semiconductor nanoparticles within LCs can be further enriched by additionally utilizing other known means, like DNA hybridization and origami-defined scaffolding that have been recently demonstrated in the nematic hosts as well [32]. Thus, the self-assembly method described here can be extended further and effectively used for the preparation of large-scale assemblies of metal and semiconductor nanostructures for the potential application in the next generation nanophotonic devices.

Funding

National Renewable Energy Laboratory; U.S. Department of Energy (DE-AC36-08GO28308).

Acknowledgments

The authors thank B. Senyuk, T. Lee, and J. Johnson for useful discussions and technical assistance.

Disclosures

The authors declare no conflicts of interest. The views expressed in the article do not necessarily represent the views of the DOE or the U.S. Government. The U.S. Government retains and the publisher, by accepting the article for publication, acknowledges that the U.S. Government retains a nonexclusive, paid-up, irrevocable, worldwide license to publish or reproduce the published form of this work, or allow others to do so, for U.S. Government purposes.

References

1. G. R. Maskaly, M. A. Petruska, J. Nanda, I. V. Bezel, R. D. Schaller, H. Htoon, J. M. Pietryga, and V. I. Klimov, "Amplified spontaneous emission in semiconductor-nanocrystal/synthetic-opal composites: optical-gain enhancement via a photonic crystal pseudogap," Adv. Mater. **18**(3), 343–347 (2006).
2. P. H. Ho, D. B. Farmer, G. S. Tulevski, S. J. Han, D. M. Bishop, L. M. Gignac, J. Bucchignano, P. Avouris, and A. L. Falk, "Intrinsically ultra-strong plasmon–exciton interactions in crystallized films of carbon nanotubes," Proc. Natl. Acad. Sci. U. S. A. **115**(50), 12662–12667 (2018).
3. M. J. Romero, J. van de Lagemaat, I. Mora-Sero, G. Rumbles, and M. M. Al-Jassim, "Imaging of resonant quenching of surface plasmons by quantum dots," Nano lett. **6**(12), 2833–2837 (2006).
4. H. Mundoor, G. H. Sheetah, S. Park, P. J. Ackerman, I. I. Smalyukh, and J. van de Lagemaat, "Tuning and switching a plasmonic quantum dot "sandwich" in a nematic line defect," ACS Nano **12**(3), 2580–2590 (2018).
5. S. J. LeBlanc, M. R. McClanahan, M. Jones, and P. J. Moyer, "Enhancement of multiphoton emission from single CdSe quantum dots coupled to gold films," Nano Lett. **13**(4), 1662–1669 (2013).
6. P. J. Ackerman, H. Mundoor, I. I. Smalyukh, and J. van de Lagemaat, "Plasmon–exciton interactions probed using spatial coentrapment of nanoparticles by topological singularities," ACS Nano **9**(12), 12392–12400 (2015).
7. H. A. Atwater and A. Polman, "Plasmonics for improved photovoltaic devices," Nat. Mater. **9**(3), 205–213 (2010).
8. I. Thomann, B. A. Pinaud, Z. Chen, B. M. Clemens, T. F. Jaramillo, and M. L. Brongersma, "Plasmon enhanced solar-to-fuel energy conversion," Nano Lett. **11**(8), 3440–3446 (2011).

Optics EXPRESS

9. A. O. Govorov, G. W. Bryant, W. Zhang, T. Skeini, J. Lee, N. A. Kotov, J. M. Slocik, and R. R. Naik, "Exciton-plasmon interaction and hybrid excitons in semiconductor-metal nanoparticle assemblies," Nano Lett. **6**(5), 984–994 (2006).
10. T. Ozel, P. L. Hernandez-Martinez, E. Mutlugun, O. Akin, S. Nizamoglu, I. Ozge Ozel, Q. Zhang, Q. Xiong, and H. V. Demir, "Observation of selective plasmon-exciton coupling in nonradiative energy transfer: Donor-selective versus acceptor-selective," Nano Lett. **13**(7), 3065–3072 (2013).
11. P. Anger, P. Bharadwaj, and L. Novotny, "Enhancement and quenching of single-molecule fluorescence," Phys. Rev. Lett. **96**(11), 113002 (2006).
12. M. Haridas, J. K. Basu, D. J. Gosztola, and G. P. Wiederrecht, "Photoluminescence spectroscopy and lifetime measurements from self-assembled semiconductor-metal nanoparticle hybrid arrays," Appl. Phys. Lett. **97**(8), 083307 (2010).
13. Y. Ofir, B. Samanta, and V. M. Rotello, "Polymer and biopolymer mediated self-assembly of gold nanoparticles," Chem. Soc. Rev. **37**(9), 1814–1825 (2008).
14. S. Srivastava, D. Nykypanchuk, M. Fukuto, J. D. Halverson, A. V. Tkachenko, K. G. Yager, and O. Gang, "Two-dimensional DNA-programmable assembly of nanoparticles at liquid interfaces," J. Am. Chem. Soc. **136**(23), 8323–8332 (2014).
15. P. G. de Gennes and J. Prost, *The Physics of Liquid Crystals* (2nd ed. Clarendo, 1993).
16. P. M. Chaikin and T. C. Lubensky, *Principles of Condensed Matter Physics* (Cambridge University, 1995).
17. B. Senyuk, J. S. Evans, P. Ackerman, T. Lee, P. Manna, L. Vigderman, E. R. Zubarev, J. van de Lagemaat, and I. I. Smalyukh, "Shape-dependent oriented trapping and scaffolding of plasmonic nanoparticles by topological defects for self-assembly of colloidal dimers in liquid crystals," Nano Lett. **12**(2), 955–963 (2012).
18. X. Wang, D. S. Miller, E. Bukusoglu, J. J. de Pablo, and N. L. Abbott, "Topological defects in liquid crystals as templates for molecular self-assembly," Nat. Mater. **15**(1), 106–112 (2016).
19. S. Park, Q. Liu, and I. I. Smalyukh, "Colloidal surfaces with boundaries, apex boojums, and nested elastic self-assembly of nematic colloids," Phys. Rev. Lett. **117**(27), 277801 (2016).
20. Q. Xu, I. Tonks, M. J. Fuerstman, J. C. Love, and G. M. Whitesides, "Fabrication of free-standing metallic pyramidal shells," Nano Lett. **4**(12), 2509–2511 (2004).
21. I. I. Smalyukh, "Liquid crystal colloids," Annu. Rev. Condens. Matter Phys. **9**(1), 207–226 (2018).
22. P. Poulin, H. Stark, T. C. Lubensky, and D. A. Weitz, "Novel colloidal interactions in anisotropic fluids," Science **275**(5307), 1770–1773 (1997).
23. H. Stark, "Physics of colloidal dispersions in nematic liquid crystals," Phys. Rep. **351**(6), 387–474 (2001).
24. P. K. Jain and M. A. El-Sayed, "Plasmonic coupling in noble metal nanostructures," Chem. Phys. Lett. **487**(4-6), 153–164 (2010).
25. A. M. Funston, C. Novo, T. J. Davis, and P. Mulvaney, "Plasmon coupling of gold nanorods at short distances and in different geometries," Nano Lett. **9**(4), 1651–1658 (2009).
26. J. J. Peterson and D. J. Nesbitt, "Modified power law behavior in quantum dot blinking: A novel role for biexcitons and Auger ionization," Nano Lett. **9**(1), 338–345 (2009).
27. A. G. Curto, G. Volpe, T. H. Taminiau, M. P. Kreuzer, R. Quidant, and N. F. van Hulst, "Unidirectional emission of a quantum dot coupled to a nanoantenna," Science **329**(5994), 930–933 (2010).
28. B. Omogo, J. F. Aldana, and C. D. Heyes, "Radiative and non-radiative lifetime engineering of quantum dots in multiple solvents by surface atom stoichiometry and ligands," J. Phys. Chem. C **117**(5), 2317–2327 (2013).
29. Q.-C. Sun, H. Mundoor, J. C. Ribot, V. Singh, I. I. Smalyukh, and P. Nagpal, "Plasmon-enhanced energy transfer for improved upconversion of infrared radiation in doped-lanthanide nanocrystals," Nano Lett. **14**(1), 101–106 (2014).
30. Q. Liu, B. Senyuk, M. Tasinkevych, and I. I. Smalyukh, "Nematic liquid crystal boojums with handles on colloidal handlebodies," Proc. Natl. Acad. Sci. U. S. A. **110**(23), 9231–9236 (2013).
31. H. Mundoor, B. Senyuk, and I. I. Smalyukh, "Triclinic nematic colloidal crystals from competing elastic and electrostatic interactions," Science **352**(6281), 69–73 (2016).
32. Q. Liu, A. Kuzyk, M. Endo, and I. I. Smalyukh, "Colloidal plasmonic DNA-origami with photo-switchable chirality in liquid crystals," Opt. Lett. **44**(11), 2831–2834 (2019).